Chemical Science

EDGE ARTICLE

View Article Online
View Journal | View Issue

Check for updates

Cite this: *Chem. Sci.*, 2019, **10**, 5801

All publication charges for this article have been paid for by the Royal Society of Chemistry

Symmetry-guided syntheses of mixed-linker Zr metal–organic frameworks with precise linker locations†

Hyehyun Kim,[a] Dongwook Kim,[a] Dohyun Moon,[b] Yong Nam Choi,[c] Seung Bin Baek *[a] and Myoung Soo Lah *[a]

Received 16th March 2019
Accepted 6th May 2019

DOI: 10.1039/c9sc01301f

rsc.li/chemical-science

While the one-pot reaction of zirconium metal ions with a mixture of two dicarboxylate heterolinkers yielded a 12-c **fcu** Zr MOF with randomly distributed linkers, the symmetry-guided stepwise reaction produced the same MOF with both linkers precisely located in the framework. In the latter method, linear terephthalic acid (H_2BDC) derivatives with *mmm* symmetry were inserted into the *mmm*-symmetry sites of the flexible Zr MOF with 8-c **bcu** topology (**ZRN-bcu**), which is composed of zigzag 2,6-naphthalenedicarboxylic acid with 2/*m* symmetry. Although the length of the symmetry-matching BDC^{2-} derivatives was much shorter than the distance between the unlinked nearest-neighbor Zr clusters in **ZRN-bcu**, induced fitting of the derivatives into the framework was possible, resulting in well-defined locations for the two different dicarboxylate linkers. Thus, controlled synthesis of MOFs with the desired topology and functionality can be achieved using a symmetry-guided approach.

Open Access Article. Published on 07 May 2019. Downloaded on 2/11/2026 10:31:31 AM.
This article is licensed under a Creative Commons Attribution-NonCommercial 3.0 Unported Licence.

Introduction

Metal–organic frameworks (MOFs) are a class of highly porous crystalline materials consisting of metal ions (or clusters) as nodes and organic ligands as linkers.[1–3] To modulate framework properties, such as pore size, shape, and surface properties, organic ligands with various functional groups are often introduced *via* either direct solvothermal reactions[4–7] or stepwise post-synthetic modifications.[6–11]

Recently, carboxylate-based Zr MOFs have received much attention owing to their improved thermal and chemical stabilities compared with those of most reported MOFs.[12] It is well known that the Zr^{4+} ion has a strong tendency to form hexanuclear $[Zr_6O_4(OH)_4(COO)_{12}]$ clusters when $[Zr_6O_4(OH)_4]^{12+}$ is fully coordinated by linear dicarboxylate ligands,[12–23] and this usually produces Zr MOFs with 12-c **fcu** topology.[12] Several UiO-66-type Zr MOFs containing two different kinds of linkers with the same length have been prepared *via* either one-pot synthesis using a mixture of heterolinkers[24,25] or post-synthetic linker exchange.[25,26] However, the linkers in these Zr MOFs are randomly distributed, and it remains a challenge to place them at specific positions in the framework.[25]

This drawback of current approaches can be overcome by performing post-synthetic insertion of secondary linkers into predetermined positions in the framework. A metal cluster with a connectivity lower than its maximum connectivity in a MOF can be further utilized as post-synthetic insertion sites for another MOF with a different net topology. From a topological point of view, the 8-c **bcu** and 12-c **fcu** topologies are similar except for the four missing equatorial linkages in the former, which generates the 8-c node.

Post-synthetic insertion of different carboxylate linkers into 8-c **bcu** Zr MOFs can give rise to 10-c, 11-c, and/or 12-c Zr MOFs with linkers positioned at specific sites in the framework.[27–29] For example, Zhou *et al.* synthesized a new Zr MOF with a 12-c hexanuclear $[Zr_6O_4(OH)_4(COO)_{12}]$ cluster *via* post-synthetic linker insertion into 8-c **bcu** PCN-700.[27] The 8-c **bcu** topology is due to steric hindrance by the methyl substituents of the 2,2′-dimethylbiphenyl-4,4′-dicarboxylate (Me_2-BPDC) linker, which forces the two carboxylate groups in a twisted conformation (Scheme 1). Because the Zr clusters alternate in two different orientations, a 12-c Zr MOF can only be obtained *via* stepwise post-synthetic insertion of both symmetry- and length-matching linear dicarboxylate linkers into PCN-700 (Scheme 1).[28] The resulting Zr MOF is an unprecedented 12-c network with the $\{3^{24}\cdot4^{28}\cdot5^{13}\cdot6\}$ point symbol.

An 8-c **bcu** Zr MOF can also be obtained by using a zigzag dicarboxylate linker with 2/*m* symmetry (Scheme 1).[30] The reduced connectivity of the Zr clusters in this Zr MOF is due to the transversal parameter of the linker, which reflects its width-

[a]*Department of Chemistry, Ulsan National Institute of Science and Technology, Ulsan 44919, Korea. E-mail: mslah@unist.ac.kr; sbbaek@unist.ac.kr*

[b]*Pohang Accelerator Laboratory, Pohang 37673, Korea*

[c]*Korea Atomic Energy Research Institute, Daejeon 34057, Korea*

† Electronic supplementary information (ESI) available: Synthesis of MOFs, PXRD, ^{1}H NMR, and crystal data. CCDC 1896107–1896112. For ESI and crystallographic data in CIF or other electronic format see DOI: 10.1039/c9sc01301f

Open Access Article. Published on 07 May 2019. Downloaded on 2/11/2026 10:31:31 AM.
This article is licensed under a Creative Commons Attribution-NonCommercial 3.0 Unported Licence.

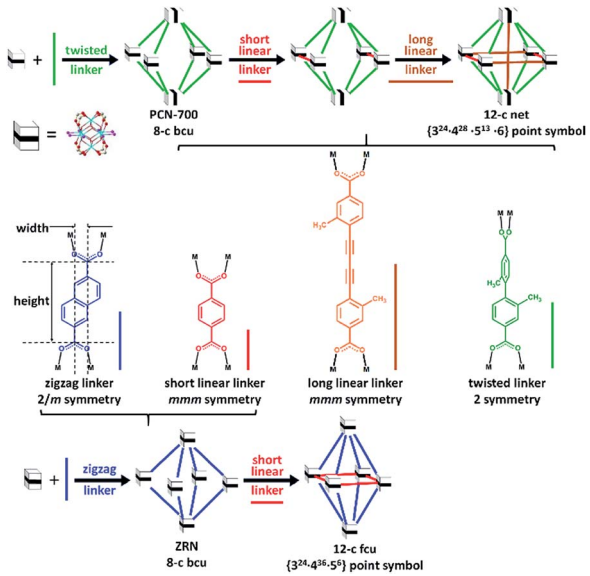

Scheme 1 Stepwise linker insertion of different types of dicarboxylate linkers to produce 12-c Zr MOFs.

to-height ratio. This Zr MOF has two sets of intercluster sites between two neighboring Zr clusters. The neighboring Zr clusters associated with the first set of intercluster sites with 2/*m* symmetry are interlinked by a zigzag linker of the same symmetry. On the other hand, the missing linkage between the other neighboring Zr clusters associated with the second set of intercluster sites is believed to be due to the mismatch between the intercluster distance and linker length. The extent of length mismatch depends on the transversal parameter of the zigzag linker, *i.e.*, the width-to-height ratio. Interestingly, a zigzag linker with a small width-to-height ratio, 2,6-naphthalenedicarboxylic acid (H_2NDC), also yielded an 8-c **bcu** Zr MOF (hereafter referred to as **ZRN-bcu**) even though the second type of intercluster distance (~8.0 Å) was only ~10% longer than the first type linked by NDC^{2-} (~7.4 Å).[29] Considering the flexibility of a framework with **bcu** topology, the missing linkage at the second type of intercluster site is probably due to symmetry mismatch and not length mismatch.

Herein, we report the symmetry-guided synthesis of such Zr MOFs using linear and zigzag dicarboxylate linkers with different symmetries and lengths whose precise locations in the framework were crystallographically determined. Post-synthetic insertion of symmetry-matching but length-mismatching linear terephthalate (H_2BDC) derivatives into the flexible **ZRN-bcu** produced a series of 12-c **fcu** Zr MOFs with two different types of ditopic heterolinkers (Scheme 1). To the best of our knowledge, this is the first report on 12-c **fcu** Zr MOFs containing two crystallographically well-defined linkers with different linker symmetries and lengths.

Results and discussion

Mixed-linker Zr-MOFs with random linker locations

Interestingly, Zr MOFs containing two dicarboxylates with different symmetries and lengths, zigzag NDC^{2-} and linear BDC^{2-}, can be prepared *via* one-pot solvothermal reactions. However, all attempts to synthesize 12-c **fcu** Zr MOFs using various ratios of the linkers produced only hybrid products (Fig. 1). The powder X-ray diffraction (PXRD) patterns of the Zr MOFs can be fitted to the same face-centered cubic lattice type, and the lattice parameters gradually decrease as the amount of the short BDC^{2-} linker increases. The linkers are not located at specific positions but randomly distributed in the framework, which accounts for the observed lattice type.

Preparation and structure of ZRN-bcu

For the synthesis of a 12-c **fcu** Zr-MOF containing two different linkers at well-defined locations *via* post-synthetic linker insertion, it is necessary to prepare an 8-c **bcu** Zr-MOF with its Zr-clusters in proper relative orientations. Because both **ZRN-bcu** and 12-c **fcu** Zr MOFs containing a zigzag NDC^{2-} linker can be prepared under similar synthetic reaction conditions, the reaction condition was modified to exclusively produce the former. The use of excess acetic acid (HAc) as the modulator produced the corresponding 12-c **fcu** Zr MOF (hereafter referred to as **ZRN-fcu**), which is also known as DUT-52.[21]

By employing trifluoroacetic acid (HTFA) as the modulator, **ZRN-bcu** crystals can be obtained under a wide range of reaction conditions (Fig. S1†). On the other hand, **ZRN-fcu** can only be obtained under very narrow reaction conditions at a 1 : 1 metal : ligand ratio and in the presence of only a small amount of HTFA. Crystallographic analysis confirmed that **ZRN-bcu** is a 3D MOF with 8-c **bcu** topology, where the cationic $[Zr_6O_4(OH)_4(COO)_8(H_2O)_8]^{4+}$ cluster on the 4/*mmm* (D_{4d}) site serves as the 8-c secondary building unit and NDC^{2-} is located on the 2/*m* (C_{2h}) site (Fig. 2a and S2†). Statistically disordered TFA counter anions are found in the solvent pore near the Zr clusters. The framework of **ZRN-bcu** is the same as that of the reported structure, $[Zr_6O_4(OH)_4(NDC)_4(H_2O)_8]^{4+}$.[29] Although **ZRN-bcu** and PCN-700 have the same topology, the arrangement of the Zr clusters in their respective frameworks is different (Fig. 2). Zr clusters in PCN-700 alternate in two different orientations since the two carboxylates of Me_2-BPDC are perpendicular to each

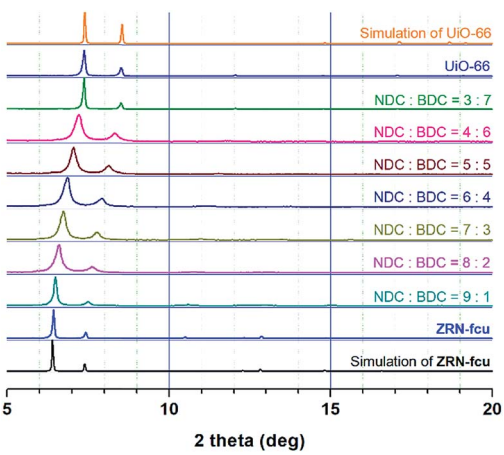

Fig. 1 PXRD patterns of a series of hybrid Zr MOFs.

This journal is © The Royal Society of Chemistry 2019

Open Access Article. Published on 07 May 2019. Downloaded on 2/11/2026 10:31:31 AM.
This article is licensed under a Creative Commons Attribution-NonCommercial 3.0 Unported Licence.

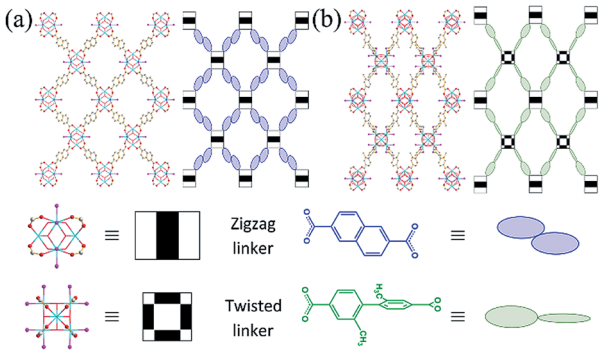

Fig. 2 Ball-and-stick models and schematic drawings of the frameworks of (a) **ZRN-bcu** and (b) PCN-700.

other (Fig. 2b). On the other hand, all Zr clusters in **ZRN-bcu** are in the same orientation owing to the coplanar conformations of the two carboxylates of NDC^{2-} (Fig. 2a). Despite the coplanarity of all potential linkage sites of the Zr clusters in **ZRN-bcu**, only a network with 8-c **bcu** topology was obtained. This preference over the 12-c **fcu** topology can be attributed to the inherent symmetry mismatch with NDC^{2-}.

Mixed-linker Zr-MOFs with precise linker locations

Although the maximum site symmetry of a dicarboxylate linker in a 12-c **fcu** Zr MOF is *mmm*, it is still possible to have only the zigzag NDC^{2-} linker of 2/*m* symmetry by using the appropriate one-pot solvothermal reaction established in this work or the previously reported one.[21] Interestingly, NDC^{2-} is statistically disordered on the *mmm*-symmetry site of the **ZRN-fcu** prepared *via* one-pot solvothermal reaction.[21] In contrast, it should be noted that the **ZRN-bcu** framework does not allow the post-synthetic incorporation of the symmetry-mismatching NDC^{2-} into the potential linkage site of *mmm* symmetry, as confirmed by all our unsuccessful attempts.

With this in mind, two different symmetries of dicarboxylate linkers were used to prepare new 12-c **fcu** Zr MOFs through post-synthetic insertion into **ZRN-bcu** (Fig. 3). To examine the effects of symmetry and length on this process, a series of symmetry-matching but length-mismatching H_2BDC derivatives (H_2XBDC) were chosen. The linker length between the carboxylic carbons (~5.4 Å) is much shorter than the ideal linker length (~8.0 Å) required to form a 12-c **fcu** Zr MOF without significant tetragonal distortion of **ZRN-bcu**.

The new Zr MOFs were obtained by soaking **ZRN-bcu** single crystals in a methanol (MeOH) solution of linear H_2XBDC (X = DO, N, and A for the $-(OH)_2$, $-NO_2$, and $-NH_2$ substituents, respectively) of *mmm* symmetry (ignoring the substituents). The replacement of the TFA counter anions in **ZRN-bcu** by $XBDC^{2-}$ was confirmed by ^1H nuclear magnetic resonance (NMR) (Fig. S3 and S4†). The ratio of NDC^{2-} to $XBDC^{2-}$ in **ZRN-NB** and **ZRN-AB** MOFs is the same as the value (2 : 1) expected from fully inserted 12-c **fcu** topology Zr MOF structures regardless of the substituent. In the case of **ZRN-DOB**, the ratio of the NDC^{2-} to DOBDC linker is about 15% smaller than the expected value, suggesting the presence of ligand-vacancy defect sites in the

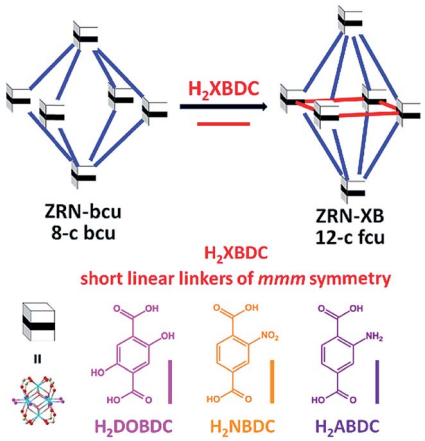

Fig. 3 Preparation of 12-c **fcu** ZRN-XB (X = DO, N, and A for the $-(OH)_2$, $-NO_2$, and $-NH_2$ substituents, respectively) *via* post-synthetic insertion of the symmetry-matching linear linker into **ZRN-bcu**.

ZRN-DOB framework. The formation of ligand-vacancy defect sites is understandable given the post-synthetic ligand insertion processes as demonstrated in sequential ligands insertions into 8-c **bcu** PCN-700 MOF.[28]

Despite the incorporation of the linear 2,5-dihydroxy-1,4-benzenedicarboxylate ($DOBDC^{2-}$) linker into the framework (as verified by the ^1H NMR spectrum), the PXRD pattern of as-synthesized **ZRN-DOB** is similar to that of as-synthesized **ZRN-bcu** (Fig. 4). Under ambient conditions, **ZRN-DOB** quickly transforms to a new crystalline phase, **ZRN-DOB-amb**, which is different from **ZRN-w** obtained from **ZRN-bcu**. On the other hand, the PXRD patterns of **ZRN-AB** and **ZRN-NB**, containing $ABDC^{2-}$ and $NBDC^{2-}$, respectively, are different from that of **ZRN-bcu** but very similar to that of **ZRN-DOB-amb** regardless of

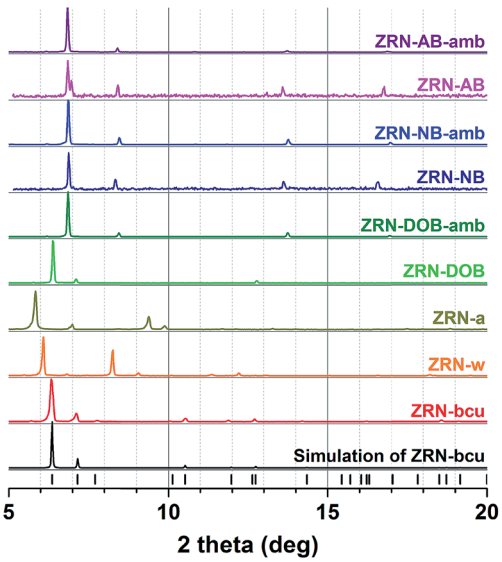

Fig. 4 PXRD patterns of **ZRN-bcu**, **ZRN-w**, **ZRN-a**, as-synthesized **ZRN-XB**, and the corresponding crystals exposed to ambient conditions.

Open Access Article. Published on 07 May 2019. Downloaded on 2/11/2026 10:31:31 AM.
This article is licensed under a Creative Commons Attribution-NonCommercial 3.0 Unported Licence.

the sample state (*i.e.*, as-synthesized crystal and crystal exposed to ambient conditions) (Fig. 4).

Because of the flexibility of the **ZRN-bcu** crystals (ESI, Fig. S5–S14†), single crystallinity during post-synthetic insertion of H_2XBDC was retained, which allowed single-crystal structure analysis. The incorporation of $DOBDC^{2-}$ into the **ZRN-bcu** framework changed the lattice type from body-centered tetragonal to primitive tetragonal. However, the unit cell parameters of **ZRN-DOB** and **ZRN-bcu** were very similar, suggesting that the insertion did not cause any significant framework distortion. Structural analysis revealed that additional $DOBDC^{2-}$ ligands are present in the framework but not inserted between the Zr clusters of the potential linkage site to form the 12-c **fcu** Zr MOF (Fig. 5 and S15†).

Two different interaction modes of the statistically disordered $DOBDC^{2-}$ ligands are therefore observed: one ligated to a Zr center in monodentate coordination mode and the other located between Zr clusters that are interconnected by an NDC^{2-} ligand. $DOBDC^{2-}$ interacts with the framework through the combination of two different weak interactions, hydrogen bonding and π–π stacking (Fig. S15†). The carboxylate oxygen atoms of $DOBDC^{2-}$ are hydrogen bonded to both the ligated water molecule and μ^3-hydroxo oxygen atom of the Zr cluster. $DOBDC^{2-}$ is further stabilized by π–π stacking interaction with NDC^{2-}.

As mentioned earlier, under ambient conditions, as-synthesized **ZRN-DOB** quickly transforms to **ZRN-DOB-amb**, which has a PXRD pattern similar to those of **ZRN-NB** and **ZRN-AB** (Fig. 4). Unfortunately, **ZRN-DOB-amb** single crystals were unsuitable for single-crystal structure analysis.

ZRN-NB can be prepared using 2-nitro-1,4-benzenedicarboxylic acid (H_2NBDC) instead of 2,5-dihydroxy-1,4-benzenedicarboxylic acid (H_2DOBDC). Induced fitting of the short $NBDC^{2-}$ linker into the potential linkage sites in **ZRN-bcu** to form 12-c **fcu** **ZRN-NB** resulted in significant tetragonal distortion of the unit cell parameters. Lattice parameters *a* and *b* shrank from 17.445 to 14.955 Å, while lattice parameter *c* elongated from 22.934 to 26.077 Å. Crystallographic analysis confirmed that **ZRN-NB** has 12-c **fcu** topology. However, the $NBDC^{2-}$ linkers at the linkage sites between the Zr clusters are ligated in a statistically disordered monodentate coordination mode rather than a bridging bidentate coordination mode (Fig. 5, 6a and b). During the insertion of $NBDC^{2-}$ into the **ZRN-bcu** framework, the conformation of the NDC^{2-} linkers in **ZRN-NB** also rotate by ~180° to relieve the steric repulsion between them, as observed in **ZRN-w** (Fig. S9†).

As-synthesized **ZRN-NB** is unstable under ambient conditions and quickly transforms to a new crystalline phase, **ZRN-NB-amb**. The two crystals have similar unit cell parameters (ESI†), as expected from the similarity of their PXRD patterns (Fig. 4). **ZRN-NB-amb** is also a 12-c **fcu** Zr MOF with two different types of dicarboxylate linkers (Fig. 5, 6c and d). However, the bridging mode of the $NBDC^{2-}$ linker with *mmm* symmetry in **ZRN-NB-amb** is different from that in **ZRN-NB**. $NBDC^{2-}$ is on an *mmm*-symmetry site in bridging bidentate coordination mode. It also induces significant tetragonal distortion of the framework, contraction of the framework in the *ab* plane, and elongation along the *c* axis. The similarity of the PXRD patterns of **ZRN-DOB-amb** and **ZRN-NB-amb** indicates that the former is also likely a 12-c **fcu** Zr MOF with $DOBDC^{2-}$ on the *mmm*-symmetry site. **ZRN-AB** single crystals containing both NDC^{2-} and $ABDC^{2-}$ linkers were also synthesized using 2-amino-1,4-benzenedicarboxylic acid (H_2ABDC) instead of H_2DOBDC *via* the same procedure to prepare **ZRN-DOB**. Structural analysis of **ZRN-AB** revealed that it is

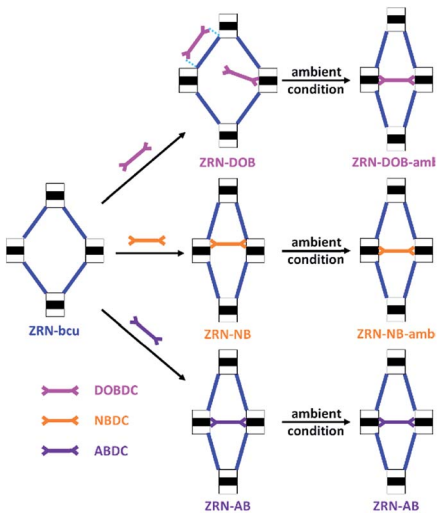

Fig. 5 Schematic drawing of the post-synthetic insertion of short linear linkers with *mmm* symmetry into the **ZRN-bcu** framework to form stable 12-c **fcu** **ZRN-XB** and **ZRN-XB-amb** under ambient conditions.

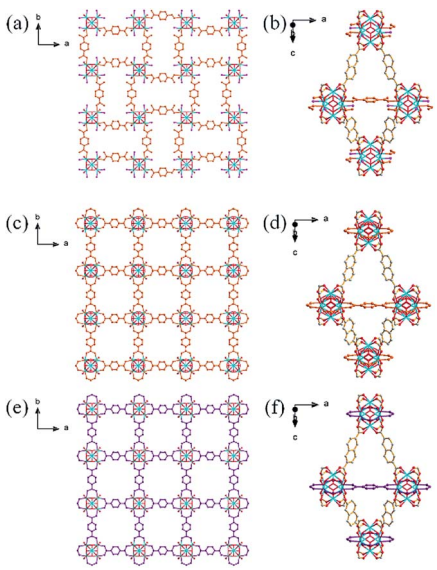

Fig. 6 Ball-and-stick diagrams of (a, b) **ZRN-NB**, (c, d) **ZRN-NB-amb**, and (e, f) **ZRN-AB**. The diagrams in (a), (c), and (e) show the connectivity and binding mode of the BDC^{2-} derivatives along the *ab* plane, while those in (b), (d) and (f) show the binding mode between nearest-neighbor Zr clusters. The statistically disordered regions and nitro and amino substituents of these linkers are omitted for clarity.

This journal is © The Royal Society of Chemistry 2019

Open Access Article. Published on 07 May 2019. Downloaded on 2/11/2026 10:31:31 AM. This article is licensed under a Creative Commons Attribution-NonCommercial 3.0 Unported Licence.

isostructural to 12-c **fcu ZRN-NB-amb**. The potential linkage sites between the Zr clusters in **ZRN-AB** are also interlinked by the $ABDC^{2-}$ linker with *mmm* symmetry in a bridging bidentate coordination mode as in 12-c **fcu ZRN-NB-amb** (Fig. 5, 6e and f). As expected, 12-c **fcu ZRN-AB** with symmetry-matching linkers on the *mmm*-symmetry sites is stable under ambient conditions.

The permanent porosities of the 12-c **fcu** Zr-MOFs, **ZRN-DOB**, **ZRN-NB** and **ZRN-AB**, were confirmed by using the N_2 sorption behaviours of their activated samples, **ZRN-DOB-a**, **ZRN-NB-a** and **ZRN-AB-a**. All the Zr-MOFs showed type-I N_2 adsorption isotherms with the Brunauer–Emmett–Teller (BET) surface areas, 1378 $m^2\ g^{-1}$, 1339 $m^2\ g^{-1}$, and 1448 $m^2\ g^{-1}$, for **ZRN-DOB-a**, **ZRN-NB-a**, and **ZRN-AB-a**, respectively (Fig. S14†). The slight variation of N_2 uptake amounts reflects the mass and size variations of the functional residues of the $XBDC^{2-}$ linkers. The N_2 adsorption amounts of the series of the 12-c **fcu MOFs** are much larger than that of the activated **ZRN-bcu** (**ZRN-a**) with short TFA linker. The BET surface area of **ZRN-a** is determined to be 861 $m^2\ g^{-1}$.

Conclusions

We demonstrated that linker symmetry can play a pivotal role in not only determining the connectivity of a metal cluster node, but also precisely locating the linkers in the framework. A Zr MOF with 12-c **fcu** topology is not a framework where a zigzag NDC^{2-} linker with 2/*m* symmetry can be inserted without causing disorder at the linker site. Careful adjustment of the reaction conditions produced **ZRN-bcu** with 8-c node containing this linker. **ZRN-bcu** has two sets of intercluster sites between two nearest-neighbor Zr clusters with different site symmetries. While the first intercluster site with 2/*m* symmetry is interconnected by the NDC^{2-} linker with the same symmetry, the second one with *mmm* symmetry remains unlinked owing to symmetry mismatch. A 12-c **fcu** Zr MOF containing both the NDC^{2-} and linear $XBDC^{2-}$ linkers at specific sites in the same framework can only be achieved by post-synthetic linker insertion into **ZRN-bcu**. Symmetry-guided insertion of $XBDC^{2-}$ with (pseudo)*mmm* point symmetry into the *mmm*-symmetry sites of **ZRN-bcu** produced a series of stable 12-c **fcu ZRN-XB** MOFs. Although the length of $XBDC^{2-}$ is much shorter than the distance between the unlinked neighboring Zr clusters in **ZRN-bcu**, the structural flexibility of the framework allowed induced fitting of the length-mismatching linker. Single-crystal structure analyses clearly showed that structural change occurred during post-synthetic linker insertion. The exact locations of the linkers in the framework were successfully defined. Symmetry-guided post-synthetic linker insertion is anticipated to become a general tool for the bottom-up synthesis of new MOFs with the desired topology and multiple functionalities in a controlled and well-defined manner.

Conflicts of interest

There are no conflicts to declare.

Acknowledgements

This work was supported by NRF (2016R1A5A1009405) through the National Research Foundation of Korea. The authors acknowledge PAL for beam line use (2018-1st-2D-029 and 2018-2nd-2d-033).

Notes and references

1 H.-C. Zhou, J. R. Long and O. M. Yaghi, *Chem. Rev.*, 2012, **112**, 673–674.
2 H. Furukawa, K. E. Cordova, M. O'Keeffe and O. M. Yaghi, *Science*, 2013, **341**, 1230444.
3 T. R. Cook, Y.-R. Zheng and P. J. Stang, *Chem. Rev.*, 2013, **113**, 734–777.
4 D. N. Bunck and W. R. Dichtel, *Chem.–Eur. J.*, 2013, **19**, 818–827.
5 J.-S. Qin, S. Yuan, Q. Wang, A. Alsalme and H.-C. Zhou, *J. Mater. Chem. A*, 2017, **5**, 4280–4291.
6 H. Deng, C. J. Doonan, H. Furukawa, R. B. Ferreira, J. Towne, C. B. Knobler, B. Wang and O. M. Yaghi, *Science*, 2010, **327**, 846–850.
7 K. Koh, J. D. Van Oosterhout, S. Toy, A. G. Wong-Foy and A. J. Matzger, *Chem. Sci.*, 2012, **3**, 2429–2432.
8 S. M. Cohen, *Chem. Rev.*, 2012, **112**, 970–1000.
9 Y. Han, J.-T. Li, Y. Xie and G. Guo, *Chem. Soc. Rev.*, 2014, **43**, 5896–5912.
10 P. Deria, J. E. Mondloch, O. Karagiaridi, W. Bury, J. T. Hupp and O. K. Farha, *Chem. Soc. Rev.*, 2014, **43**, 5896–5912.
11 O. Karagiaridi, W. Bury, J. E. Mondloch, J. E. Hupp and O. K. Farha, *Angew. Chem., Int. Ed.*, 2014, **53**, 4530–4540.
12 Y. Bai, Y. Dou, L.-H. Xie, W. Rutledge, J.-R. Li and H.-C. Zhou, *Chem. Soc. Rev.*, 2016, **45**, 2327–2367.
13 J. H. Cavka, S. Jakobsen, U. Olsbye, N. Guillou, C. Lamberti, S. Bordiga and K. P. Lillerud, *J. Am. Chem. Soc.*, 2008, **130**, 13850–13851.
14 S. J. Garibay and S. M. Cohen, *Chem. Commun.*, 2010, **46**, 7700–7702.
15 A. Schaate, P. Roy, A. Godt, J. Lippke, F. Waltz, M. Wiebcke and P. Behrens, *Chem.–Eur. J.*, 2011, **17**, 6643–6651.
16 H.-L. Jiang, D. Feng, T.-F. Liu, J.-R. Li and H.-C. Zhou, *J. Am. Chem. Soc.*, 2012, **134**, 14690–14693.
17 L. Li, S. Tang, C. Wang, X. Lv, M. Jiang, H. Wu and X. Zhao, *Chem. Commun.*, 2014, **50**, 2304–2307.
18 C. Wang, O. Volotskova, K. Lu, M. Ahmad, C. Sun, L. Xing and W. Lin, *J. Am. Chem. Soc.*, 2014, **136**, 6171–6174.
19 R. J. Marshall, S. L. Griffin, C. Wilson and R. S. Forgan, *J. Am. Chem. Soc.*, 2015, **137**, 9527–9530.
20 G. Wißmann, A. Schaate, S. Lilienthal, I. Bremer, A. M. Schneider and P. Behrens, *Microporous Mesoporous Mater.*, 2012, **152**, 64–70.
21 V. Bon, I. Senkovska, M. S. Weiss and S. Kaskel, *CrystEngComm*, 2013, **15**, 9572–9577.
22 B. Wang, H. Huang, X.-L. Lv, Y. Xie, M. Li and J. R. Li, *Inorg. Chem.*, 2014, **53**, 9254–9259.

Open Access Article. Published on 07 May 2019. Downloaded on 2/11/2026 10:31:31 AM.
This article is licensed under a Creative Commons Attribution-NonCommercial 3.0 Unported Licence.

23 K. Wang, H. Huang, W. Xue, D. Liu, X. Zhao, Y. Xiao, Z. Li, Q. Yang, L. Wang and C. Zhong, *CrystEngComm*, 2015, **17**, 3586–3590.
24 M. Kim, J. F. Cahill, K. A. Prather and S. M. Cohen, *Chem. Commun.*, 2011, **47**, 7629–7631.
25 W. Schrimpf, J. Jiang, Z. Ji, P. Hirschle, D. C. Lamb, O. M. Yaghi and S. Wuttke, *Nat. Commun.*, 2018, **9**, 1647.
26 M. Kim, J. F. Cahill, Y. Su, K. A. Prather and S. M. Cohen, *Chem. Sci.*, 2012, **3**, 126–130.
27 S. Yuan, W. Lu, Y.-P. Chen, Q. Zhang, T.-F. Liu, D. Feng, X. Wang, J. Qin and H.-C. Zhou, *J. Am. Chem. Soc.*, 2015, **137**, 3177–3180.
28 S. Yuan, Y.-P. Chen, J.-S. Qin, W. Lu, L. Zou, Q. Zhang, X. Wang, X. Sun and H.-C. Zhou, *J. Am. Chem. Soc.*, 2016, **138**, 8912–8919.
29 C.-X. Chen, Z. Wei, J.-J. Jiang, Y.-Z. Fan, S.-P. Zheng, C.-C. Cao, Y.-H. Li, D. Fenske and C.-Y. Su, *Angew. Chem., Int. Ed.*, 2016, **55**, 9932–9936.
30 V. Guillerm, T. Grancha, I. Imaz, J. Juanhuix and D. Maspoch, *J. Am. Chem. Soc.*, 2018, **140**, 10153–10157.

This journal is © The Royal Society of Chemistry 2019